SUPPLEMENTARY MATERIALS: A METHOD TO COARSE-GRAIN MULTI-AGENT STOCHASTIC SYSTEMS WITH REGIONS OF MULTISTABILITY*

DARIA STEPANOVA†, HELEN M. BYRNE‡, PHILIP K. MAINI‡, AND TOMÁS ALARCÓN§

SM1. VEGF-Delta-Notch system. The VEGF-Delta-Notch signalling pathway mediates phenotype specification of endothelial cells (ECs) during angiogenesis and vasculogenesis [SM1, SM4]. In a two-dimensional geometry, lateral inhibition induced by Delta-Notch trans-interactions (i.e. binding of a Delta ligand on one cell to a Notch receptor on a neighbouring EC) produces an alternating pattern of cells with two distinct levels of gene expression which correspond to 'Delta-high' and 'Delta-low' phenotypes (in angiogenesis, the Delta-high (Delta-low) phenotype is referred to as tip (stalk) cell) [SM8, SM11]. Delta-high cells are characterised by elevated levels of Delta ligand and VEGFR2 (VEGF receptor 2), and low levels of Notch, whereas Delta-low cells are associated with low levels of Delta and VEGFR2, and high levels of Notch. When Delta-Notch signalling is combined with cell activation in response to extracellular VEGF stimulation, the robustness of the cell phenotypes increases [SM2].

SM1.1. Individual cell system. A schematic of the kinetic reactions involved in the VEGF-Delta-Notch signalling pathway for an individual cell system is shown in Figure SM1. Briefly, a Notch receptor trans-binds a Delta ligand on a neighbouring cell (reaction (1a) in Figure SM1). This leads to cleavage of the Notch Intracellular Domain (NICD) which, on translocation to the nucleus, inhibits (gene) expression of VEGFR2 (reaction (2)) and up-regulates (gene) expression of the Notch receptor (reaction (3)). After trans-binding, the Delta ligand is degraded or recycled by endocytosis (reaction (1b)). Delta-Notch interactions can also occur on the membrane of the same cell, via a phenomenon termed cis-inhibition, which inhibits Delta and Notch from interacting with other proteins until they are eventually degraded (reaction (4)). At the same time, VEGF, on binding to its receptor, VEGFR2, activates this receptor (reaction (5)) which up-regulates production of Delta ligand (reaction (6)). The model also accounts for degradation of all proteins (see, for example, reaction (7) for NICD degradation).

Zooming out from the detailed description of each kinetic reaction, we note that trans-activation of Notch in a focal cell by Delta ligand from a neighbouring cell (production of an NICD) produces a positive feedback for Notch expression and negative feedback for Delta production. Thus, a focal cell with low levels of Delta expression can down-regulate Notch levels in fewer neighbouring cells while being further

*Supplementary material for MMS MS#M141857.
https://doi.org/10.1137/21M1418575

†Centre de Recerca Matemàtica, Bellaterra (Barcelona) 08193, Spain, and Departament de Matemàtiques, Universitat Autònoma de Barcelona, Bellaterra (Barcelona) 08193, Spain (dstepanova@crm.cat).

‡Wolfson Centre for Mathematical Biology, Mathematical Institute, University of Oxford, Oxford OX2 6GG, UK (Helen.Byrne@maths.ox.ac.uk, Philip.Maini@maths.ox.ac.uk).

§Institució Catalana de Recerca i Estudis Avançats (ICREA), Barcelona 08010, Spain, Centre de Recerca Matemàtica, Bellaterra (Barcelona) 08193, Spain, and Departament de Matemàtiques, Universitat Autònoma de Barcelona, Bellaterra (Barcelona) 08193, Spain (talarcon@crm.cat).

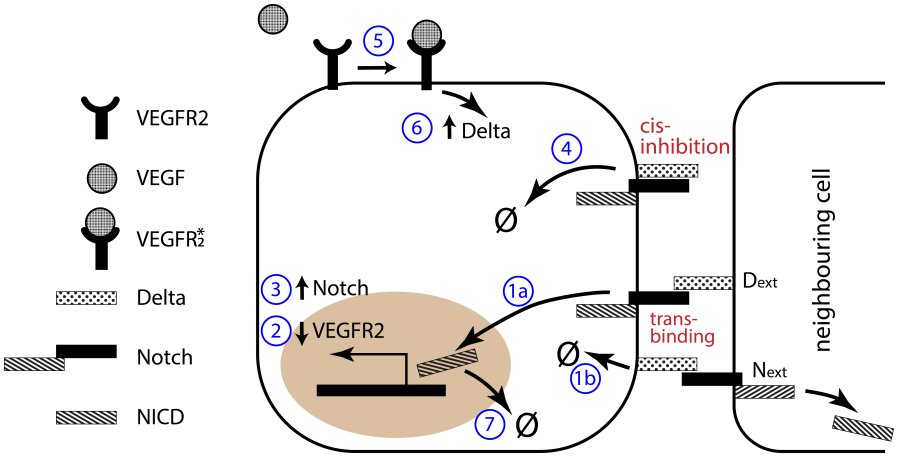

FIG. SM1. ***A schematic of the kinetic reactions incorporated in our mathematical model of the VEGF-Delta-Notch signalling pathway for the individual cell system [SM9].*** *The reactions are labelled by blue circled numbers (see Table SM2). N_{ext} and D_{ext} represent extracellular levels of Notch and Delta, respectively. $VEGFR_2^*$ denotes VEGFR2 receptor activated by extracellular VEGF.*

TABLE SM1

Dependent variables associated with our model of the VEGF-Delta-Notch signalling pathway. *Capital letters indicate numbers of protein molecules (used in the full stochastic system), while lowercase letters represent the corresponding dimensionless protein concentrations (used in the mean-field system of equations).*

Protein	**Dependent variable (dimensional)**	**Concentration (dimensionless)**
Notch receptor	N	n
Delta ligand	D	d
NICD	I	ι
VEGFR2	R_2	r_2
activated (bound to VEGF) VEGFR2	R_2^*	r_2^*

inhibited by its neighbours due to its up-regulated Notch level. This mechanism of crosstalk between cells (when ligand, here Delta, on one cell inhibits production of the same ligand in neighbours) is known as lateral inhibition. We refer to our previous work [SM9] in which we presented a detailed derivation and analysis of the kinetic reactions and the corresponding mean-field equations for this signalling pathway. Here we list the kinetic reactions and the corresponding transition rates of the full stochastic continuous time Markov chain (CTMC) model and its deterministic mean-field limit. The dependent variables and their non-dimensional concentrations are listed in Table SM1. Given the size of the stochastic system, Ω, we relate the number of molecules of a protein, P, with its non-dimensional concentration, p, via $p = {}^{P}/_{\Omega}$.

Given the transition rates and the corresponding stoichiometric vectors (listed in Table SM2), we can formulate our individual cell stochastic model of the VEGF-Delta-Notch pathway in terms of the Chemical Master Equation (CME)

TABLE SM2

Details of the kinetic reactions included in our full stochastic model of the VEGF-Delta-Notch signalling pathway within an individual cell. *Here* $H^S\left(S; S_0, \lambda_{S,P}, n_P\right) = \frac{1+\lambda_{S,P}\left({}^{S}/_{S_0}\right)^{n_P}}{1+\left({}^{S}/_{S_0}\right)^{n_P}}$ *is the so-called shifted Hill function. It represents the regulation of gene expression of protein,* P*, in response to the signalling variable,* S*. Production of* P *is down-regulated (up-regulated) for* $0 \leq \lambda_{S,P} < 1$ *(*$\lambda_{S,P} > 1$*) as the level of signal,* S*, grows. The prefactor in front of* $H^S(\cdot;\cdot,\cdot,\cdot)$ *indicates the baseline production of the corresponding protein.* N_{ext} *and* D_{ext} *represent extracellular levels of Notch and Delta, respectively, which are fixed model parameters for the individual cell system. A full list of parameter values is given in Table* SM3*.* Ω *represents system size, which is used to scale the transition rates [SM5]. The stoichiometric vectors,* ν_r*, are indexed as* $(N, D, I, R_2, R_2^*)^T$*. Reaction labels are as in Figure* SM1*.*

Reaction label, r	**Kinetic reaction(s)**	**Transition rate(s),** α_r	**Stoichiometric vector(s),** ν_r
(1a)	$N+D_{ext} \longrightarrow I+D_{ext}$	$d_{ext}N$, $d_{ext} = {}^{D_{ext}}/_{\Omega}$	$(-1,0,+1,0,0)^T$
(1b)	$D + N_{ext} \longrightarrow N_{ext}$	$\eta n_{ext} D$, $n_{ext} = {}^{N_{ext}}/_{\Omega}$	$(0,-1,0,0,0)^T$
(2)	$\emptyset \rightleftarrows R_2$	$[\rightarrow]\, \Omega\beta_{R_2} H^S(\rho_N I; \Omega, \lambda_{I,R_2}, n_{R_2})$ $[\leftarrow]\, R_2$	$(0,0,0,+1,0)^T$ $(0,0,0,-1,0)^T$
(3)	$\emptyset \rightleftarrows N$	$[\rightarrow]\, \Omega\beta_N H^S(\rho_N I; \Omega, \lambda_{I,N}, n_N)$ $[\leftarrow]\, N$	$(+1,0,0,0,0)^T$ $(-1,0,0,0,0)^T$
(4)	$N + D \longrightarrow \emptyset$	$\frac{\kappa}{\Omega} ND$	$(-1,-1,0,0,0)^T$
(5)	$R_2 \longrightarrow R_2^*$ $R_2^* \longrightarrow \emptyset$	$v_{ext} R_2$ τR_2^*	$(0,0,0,-1,+1)^T$ $(0,0,0,0,-1)^T$
(6)	$\emptyset \rightleftarrows D$	$[\rightarrow]\, \Omega\beta_D H^S(\rho_{R_2} R_2^*; \Omega, \lambda_{R_2^*,D}, n_D)$ $[\leftarrow]\, D$	$(0,+1,0,0,0)^T$ $(0,-1,0,0,0)^T$
(7)	$I \longrightarrow \emptyset$	τI	$(0,0,-1,0,0)^T$

$$\frac{\partial \mathrm{P}(X,t)}{\partial t} = \sum_r \left(\alpha_r(X-\nu_r)\,\mathrm{P}(X-\nu_r,t) - \alpha_r(X,t)\,\mathrm{P}(X,t)\right), \tag{SM1.1}$$

where $X = (N, D, I, R_2, R_2^*)^T$ and $\mathrm{P}(X,t)$ is the probability of finding the system in state X at time t. This CME cannot be solved analytically but can be numerically simulated via the Gillespie algorithm (GA) [SM5] or the more efficient Next Subvolume (NSV) method [SM3]. The computational cost of these simulations rapidly increases with the system size, Ω. Furthermore, when extended to a multicellular system, the simulation time increases as the number of cells in the system increases (linearly for the GA or logarithmically for the NSV method). Thus, high computational power is required to perform numerical simulations for large numbers of cells ($O(10^2)-O(10^3)$) as in the angiogenesis model (see Figures 14a and 14b, left panels).

We can significantly decrease the computational cost of model simulations by deriving the mean-field limit equations, which read:

$$\begin{aligned}
\frac{\mathrm{d}n}{\mathrm{d}t} &= \beta_N H^S(\rho_N \iota; 1.0, \lambda_{I,N}, n_N) - n - d_{ext}\, n - \kappa n d,\\
\frac{\mathrm{d}d}{\mathrm{d}t} &= \beta_D H^S(\rho_{R_2} r_2^*; 1.0, \lambda_{R_2^*,D}, n_D) - d - \eta n_{ext}\, d - \kappa n d,
\end{aligned}$$

(SM1.2)
$$\begin{aligned}\frac{\mathrm{d}\iota}{\mathrm{d}t} &= d_{ext}\, n - \tau\, \iota,\\ \frac{\mathrm{d}r_2}{\mathrm{d}t} &= \beta_{R_2} H^S(\rho_N \iota; 1.0, \lambda_{I,R_2}, n_{R_2}) - (1 + v_{ext}) r_2,\\ \frac{\mathrm{d}r_2^*}{\mathrm{d}t} &= v_{ext}\, r_2 - \tau\, r_2^*.\end{aligned}$$

This system of equations is bistable for a range of values of the control (bifurcation) parameters, here the extracellular Delta and Notch concentrations, d_{ext} and n_{ext}, respectively [SM9]. In Figure SM2a, we present a bifurcation diagram showing how the steady state non-dimensional Notch concentration, n, changes as d_{ext} varies for a fixed value of n_{ext}. We note that for low (high) values of d_{ext}, the system is monostable, its only stable steady state corresponding to the Delta-high (Delta-low) cell phenotype. For intermediate values of d_{ext}, the system has two stable steady states (i.e. in this region both phenotypes coexist).

The mean-field equations (Equation (SM1.2)) are valid in the limit $\Omega \to \infty$. For finite values of Ω (as in any biological system), some level of noise is always present. This can affect the dynamics of the system, leading to behaviours which differ from the mean-field limit. In Figure SM2b, we plot the non-dimensional Notch concentration of an individual cell during a single realisation of our multiscale model of angiogenesis [SM9]. Arrows on this plot indicate times at which the focal cell switched its phenotype. For example, a phenotype switch from Delta-low to Delta-high cell at $t = 478$ minutes indicates that, during the simulation, the neighbourhood of the focal cell ($\{d_{ext}, n_{ext}\}$) changed and the cell was forced to adjust its phenotype accordingly.

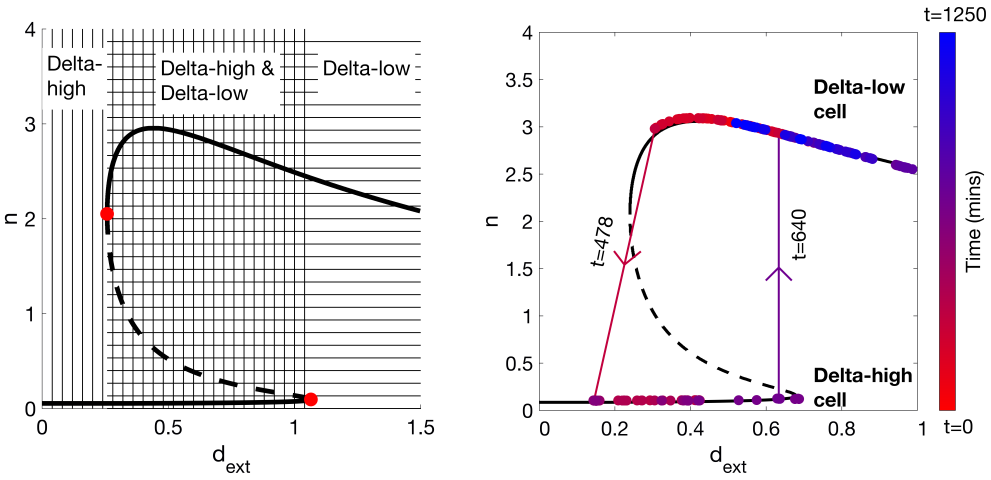

(a) (b)

FIG. SM2. *(a) A bifurcation diagram (corresponding to Equation (SM1.2)) for the non-dimensional Notch concentration, n, as a function of extracellular Delta signalling, d_{ext}. The solid lines correspond to stable steady states; dashed line - to unstable saddle points. Saddle-node bifurcation points are indicated by red filled circles. Vertical (horizontal) hatching indicates a region in which the Delta-high (Delta-low) cell steady state exists. (b) Notch concentration, n, of a representative cell during simulation of a multiscale angiogenesis model [SM9] as the function of the cell's extracellular Delta signal, d_{ext}. The black line corresponds to a bifurcation curve (as in (a)) for a fixed value of n_{ext} (although this value changes together with d_{ext} in the simulations of our angiogenesis model, the bifurcation curve does not change significantly, so just one of them was plotted for simplicity). Arrows indicate phenotype switch transitions for the representative cell with the corresponding times. The colour bar represents simulation time.*

However, the phenotype switch, from Delta-high to Delta-low cell, at $t = 640$ minutes is noise-induced since the cell's neighbourhood (i.e. d_{ext}) did not change at that time. Phenotype transitions of this type cannot be accounted for by the deterministic mean-field model. Likewise, Figure SM2b confirms that fluctuations away from the mean-field steady state values are small since the simulated trajectory of the focal cell (circled markers) lies in a narrow neighbourhood around the deterministic bifurcation curve. This strengthens the case for the application of large deviation theory to coarse-grain the dynamics of this system.

SM1.2. Multicellular system. In order to extend the individual cell CTMC model of the VEGF-Delta-Notch system given by the CME, Equation (SM1.1), and the corresponding kinetic reactions listed in Table SM2, to a multicellular system in a 2D domain, we need only to specify the external levels of Delta, $(D_{ext})_k$, and Notch, $(N_{ext})_k$ (for the mean-field model, $(d_{ext})_k$ and $(n_{ext})_k$, respectively) for a cell situated in voxel k. A key parameter to determine cell cross-talk is the cell interaction radius, R_s, allowing for non-local (beyond immediate neighbours on a chosen lattice) interactions between cells. This is because in this model, cell position is known up to the position of its nucleus, and cell interactions are assumed to occur via membrane protrusions within a circular neighbourhood of its nucleus. Thus, $(D_{ext})_k$ and $(N_{ext})_k$ are computed as a normalised sum of the corresponding protein over all the neighbouring ECs within the interaction radius, R_s, from the focal cell's nucleus (for more details, see [SM9]):

$$(D_{ext})_k = \sum_{v_l \,\in\, neighbours(k)} \alpha_{kl} D_l, \tag{SM1.3a}$$

$$(N_{ext})_k = \sum_{v_l \,\in\, neighbours(k)} \alpha_{kl} N_l. \tag{SM1.3b}$$

Here k indicates the voxel index of the multicellular system. The weight $\alpha_{kl} = \frac{|v_l \cap \mathcal{B}_{R_s}(k)|}{A(k)}$, with $A(k) = \sum_j |v_j \cap \mathcal{B}_{R_s}(k)|$, represents the proportion of the area of the circular neighbourhood of radius R_s surrounding the focal cell in voxel v_k, $\mathcal{B}_{R_s}(k)$, that overlaps with voxel v_l.

When a bimolecular reaction of Delta-Notch trans-binding occurs, the neighbouring cell (in $neighbours(k)$) is chosen probabilistically (reaction (1a); reaction (1b) is redundant for multicellular systems since it is accounted for as reaction (1a) which takes place in neighbouring cells).

The derivation of the mean-field system is straightforward. For each voxel, v_k, in the lattice we specify a system of ODEs:

$$\begin{aligned}
\frac{\mathrm{d}n_k}{\mathrm{d}t} &= \beta_N H^S(\rho_N \iota_k; 1.0, \lambda_{I,N}, n_N) - n_k - (d_{ext})_k \, n_k - \kappa n_k d_k, \\
\frac{\mathrm{d}d_k}{\mathrm{d}t} &= \beta_D H^S(\rho_{R_2} \, (r_2^*)_k \, ; 1.0, \lambda_{R_2^*,D}, n_D) - d_k - \eta \, (n_{ext})_k \, d_k - \kappa n_k d_k, \\
\frac{\mathrm{d}\iota_k}{\mathrm{d}t} &= (d_{ext})_k \, n_k - \tau \, \iota_k, \\
\frac{\mathrm{d}\,(r_2)_k}{\mathrm{d}t} &= \beta_{R_2} H^S(\rho_N \iota_k; 1.0, \lambda_{I,R_2}, n_{R_2}) - (1 + v_{ext}) \, (r_2)_k \, , \\
\frac{\mathrm{d}\,(r_2^*)_k}{\mathrm{d}t} &= v_{ext} \, (r_2)_k - \tau \, (r_2^*)_k \, ,
\end{aligned} \tag{SM1.4}$$

$$(d_{ext})_k = \sum_{v_l \in \, neighbours(k)} \alpha_{kl} d_l,$$
$$(n_{ext})_k = \sum_{v_l \in \, neighbours(k)} \alpha_{kl} n_l.$$

Here, again, cross-talk between neighbouring cells is accounted for via $(d_{ext})_k$ and $(n_{ext})_k$.

SM2. Geometric minimum action method (gMAM). The geometric minimum action method (gMAM) was developed in [SM7] as a technique for efficient numerical computation of the minimum action path (MAP) and the corresponding quasipotential (given as the minimum of the action functional) of a rare event. Briefly, starting with the geometric representation, $\widehat{S}(\phi)$ (Equation (2.6)), the Euler-Lagrange equation associated with the minimisation of $\widehat{S}(\phi)$ is derived, assuming $\hat{\theta}(\phi, \phi')$ is known. Then a (pre-conditioned) steepest descend algorithm can be used to solve this Euler-Lagrange equation, maintaining the standard arc length parametrisation of ϕ. If no explicit formula for $\hat{\theta}(\phi, \phi')$ is available, then $\hat{\theta}(\phi, \phi')$ is computed in the inner loop of the algorithm, as a solution to the system

$$H(x, \hat{\theta}) = 0 \tag{SM2.1a}$$
$$\frac{\partial H(x, \theta)}{\partial \theta} = \lambda \phi' \tag{SM2.1b}$$

for some λ.

For a diffusion process of type Equation (2.1), there are explicit expressions for the Lagrangian and the corresponding Hamiltonian

$$L(x, y) = \langle y - b(x), a^{-1}(x)(y - b(x)) = \|y - b(x)\|_a^2, \tag{SM2.2a}$$
$$H(x, \theta) = \langle b(x), \theta \rangle + \frac{1}{2} \langle \theta, a(x)\theta \rangle, \tag{SM2.2b}$$

where $\|p\|_a^2 = \langle p, a^{-1}(x)\ p \rangle^{1/2}$ is a norm induced by the diffusion tensor, $a(x)$. This allows us to explicitly derive the action functional in its geometric reformulation [SM7],

$$\widehat{S}(\phi) = \left(\int_0^1 \|\phi'\|_a \|b(\phi)\|_a - \langle \phi', a^{-1}(\phi) b(\phi) \rangle \right) d\alpha,$$

and the solution to the system of equations Equation (SM2.1):

$$\hat{\theta}(x, y) = a^{-1}(x) \left(\frac{\|b(x)\|_a}{\|y\|_a} - b(x) \right), \tag{SM2.3a}$$
$$\lambda(x, y) = \frac{\|b(x)\|_a}{\|y\|_a}. \tag{SM2.3b}$$

For a general birth-death CTMC of type Equation (SM1.1) with transition rates, $\alpha_r(x)$, and the corresponding stoichiometric vectors, ν_r, the Hamiltonian reads:

$$H(x, \theta) = \sum_r \alpha_r(x) \left(\exp\left(\langle \theta, \nu_r \rangle \right) - 1 \right). \tag{SM2.4}$$

In this case, there is no explicit solution to the system given by Equation (SM2.1) but it can be computed in the inner loop of the gMAM [SM7].

For the convergence of the gMAM for an SDE, a and b must be bounded and uniformly continuous, and a has to be uniformly elliptic, whereas, for a CME, the rate functions, α_r, must be uniformly bounded away from 0 and $+\infty$ [SM7].

For alternative numerical methods to compute minimum action paths (MAPs) we refer the reader to [SM6, SM10] and references therein.

SM3. System of stochastic differential equations of the VEGF-Delta-Notch model (individual cell). Let $x^\epsilon = (n^\epsilon, d^\epsilon, \iota^\epsilon, r_2^\epsilon, r_2^{*\epsilon})^T$. Then, the SDE for the stochastic VEGF-Delta-Notch system reads:

$$\mathrm{d}x^\epsilon(t) = b(x^\epsilon)\mathrm{d}t + \sqrt{\epsilon}\sigma(x^\epsilon)\mathrm{d}W. \tag{SM3.1}$$

Here the drift vector, $b(x^\epsilon) \in \mathrm{R}^5$, is given by Equation (SM3.2), the diffusion tensor, $a(x^\epsilon) = (\sigma\sigma^T)(x^\epsilon) \in \mathrm{R}^{5\times5}$, and $\sigma^T(x^\epsilon) \in \mathrm{R}^{12\times5}$ is given by Equation (SM3.3). The level of noise is controlled by $\epsilon = \Omega^{-1}$. Finally, W is a Wiener process in R^{12}.

$$b(x^\epsilon) = \begin{pmatrix} \beta_N H^S(\rho_N \iota^\epsilon; 1.0, \lambda_{I,N}, n_N) - n^\epsilon - d_{ext}\, n^\epsilon - \kappa n^\epsilon d^\epsilon \\ \beta_D H^S(\rho_{R_2} r_2^{*\epsilon}; 1.0, \lambda_{R_2^*,D}, n_D) - d^\epsilon - \eta n_{ext}\, d^\epsilon - \kappa n^\epsilon d^\epsilon \\ d_{ext}\, n^\epsilon - \tau\, \iota^\epsilon \\ \beta_{R_2} H^S(\rho_N \iota^\epsilon; 1.0, \lambda_{I,R_2}, n_{R_2}) - (1 + v_{ext}) r_2^\epsilon \\ v_{ext}\, r_2^\epsilon - \tau\, r_2^{*\epsilon} \end{pmatrix}. \tag{SM3.2}$$

Here the shifted Hill function, $H^S(p; p_0, \lambda, n) = \frac{1+\lambda\left({}^{p}/_{p_0}\right)^n}{1+\left({}^{p}/_{p_0}\right)^n}$.

The matrix $\sigma^T(x^\epsilon)$ takes the form:

$$\sigma^T(x^\epsilon) = \begin{pmatrix} S_1(x^\epsilon) & 0_{8\times2} \\ 0_{4\times3} & S_2(x^\epsilon) \end{pmatrix}, \tag{SM3.3}$$

where $0_{n\times m}$ is a zero block matrix of size $n \times m$, and block matrices $S_1(x^\epsilon) \in \mathrm{R}^{8\times5}$ and $S_2(x^\epsilon) \in \mathrm{R}^{4\times2}$ are defined as

$$S_1(x^\epsilon) = \begin{pmatrix} \sqrt{\beta_N H^S(\rho_N \iota^\epsilon; 1.0, \lambda_{I,N}, n_N)} & 0 & 0 \\ -\sqrt{n^\epsilon} & 0 & 0 \\ 0 & \sqrt{\beta_D H^S(\rho_{R_2} r_2^{*\epsilon}; 1.0, \lambda_{R_2^*,D}, n_D)} & 0 \\ 0 & -\sqrt{d^\epsilon} & 0 \\ -\sqrt{d_{ext}\, n^\epsilon} & 0 & \sqrt{d_{ext}\, n^\epsilon} \\ 0 & -\sqrt{\eta n_{ext}\, d^\epsilon} & 0 \\ 0 & 0 & -\sqrt{\tau r_2^{*\epsilon}} \\ -\sqrt{\kappa n^\epsilon d^\epsilon} & -\sqrt{\kappa n^\epsilon d^\epsilon} & 0 \end{pmatrix},$$

$$S_2(x^\epsilon) = \begin{pmatrix} \sqrt{\beta_{R_2} H^S(\rho_N \iota^\epsilon; 1.0, \lambda_{I,R_2}, n_{R_2})} & 0 \\ -\sqrt{v_{ext}\, r_2^\epsilon} & -\sqrt{v_{ext}\, r_2^\epsilon} \\ -\sqrt{r_2^\epsilon} & 0 \\ 0 & -\sqrt{r_2^{*\epsilon}} \end{pmatrix}.$$

SM4. Minimum action path (MAP) for the VEGF-Delta-Notch system in an individual cell. Using the SDE for the VEGF-Delta-Notch system (Equations (SM3.1)–(SM3.3)), we implemented the gMAM to compute the minimum action path (MAP) and the corresponding quasipotential (using explicit expressions for the Hamiltonian and the momentum, Equations (SM2.2) and (SM2.3)). An illustration of the MAPs for transitions between phenotypes for a fixed set of parameters (Table SM3) is shown in Figure SM3. In addition, Figure SM4 demonstrates the tubular neighbourhoods around these MAPs (the transition tubes within which phenotype transitions occur) for different values of the noise level. In can be seen that transition paths can diverge more from the corresponding MAP in higher noise levels ($\epsilon \approx 0.014$ in Figure SM4a) than in lower ones ($\epsilon \approx 0.002$ in Figure SM4b).

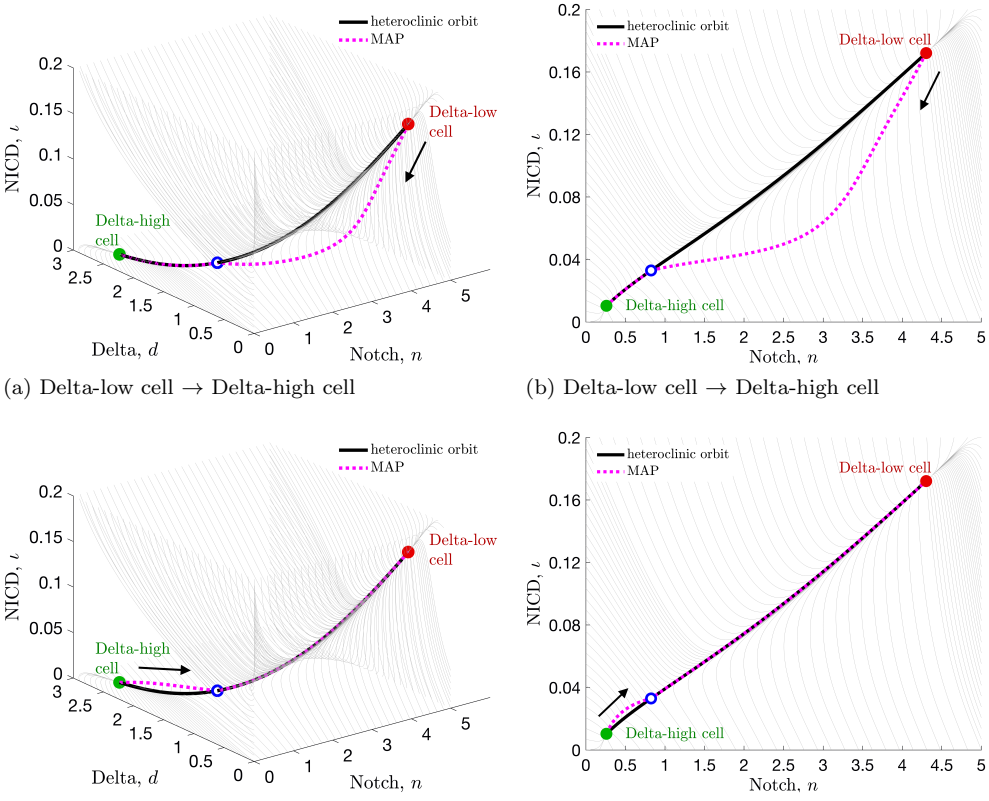

(a) Delta-low cell → Delta-high cell

(b) Delta-low cell → Delta-high cell

(c) Delta-high cell → Delta-low cell

(d) Delta-high cell → Delta-low cell

FIG. SM3. ***Minimum action paths.*** *Projections (3D, left panels; 2D, right panels) of the MAPs computed using the gMAM (dotted magenta lines) for transitions from (a)-(b) Delta-low cell → Delta-high cell; (c)-(d) Delta-high cell → Delta-low cell. Streamlines associated with the mean-field model are drawn in grey. Stable steady states corresponding to Delta-high (Delta-low) phenotype are indicated by filled green (red) circles; unstable saddle points are indicated by unfilled blue circles. Heteroclitic orbits, connecting steady states, are indicated by thick black lines.*

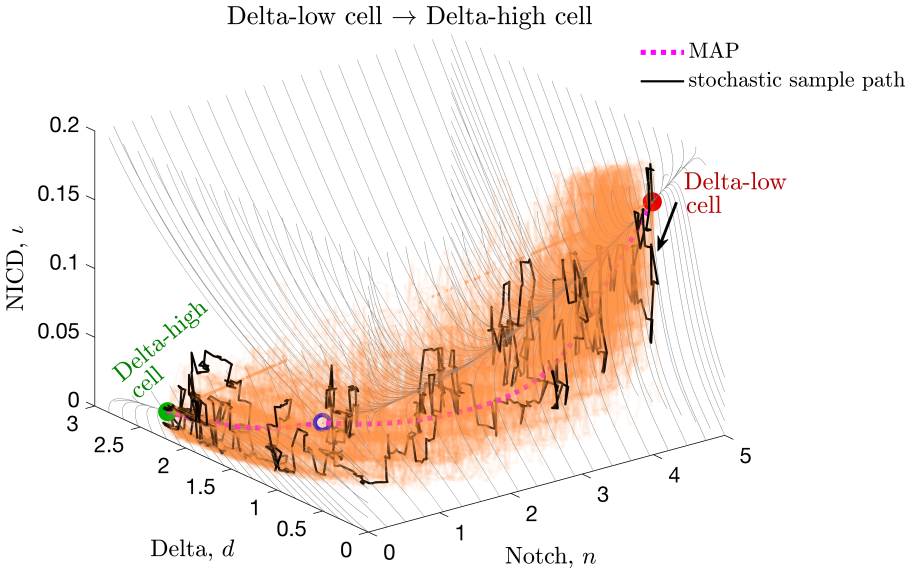

(a) system size, $\Omega = 70$ (noise level, $\epsilon = 1/\Omega \approx 0.014$)

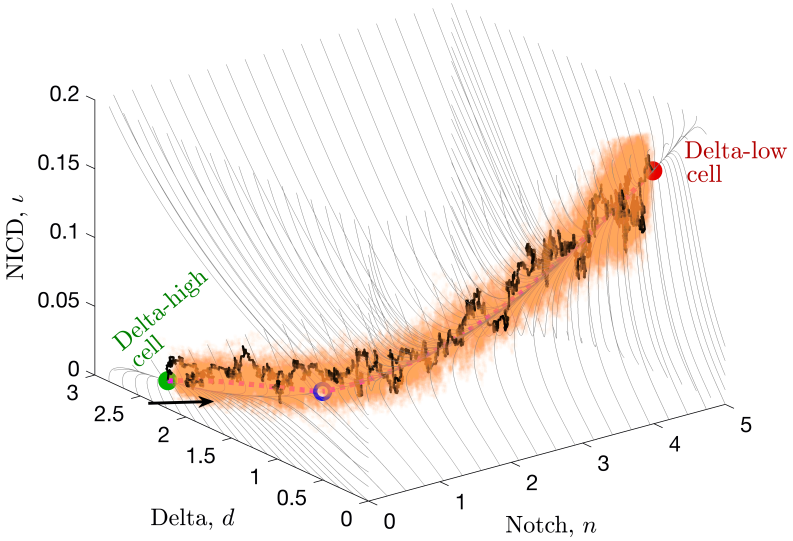

(b) system size, $\Omega = 450$ (noise level, $\epsilon = 1/\Omega \approx 0.002$)

FIG. SM4. ***An illustration of the transition tubes for stochastic sample paths of transitions between the cell phenotypes.*** *This figure corresponds to Figure 5 of the main text. Here, we additionally plotted in orange* 100 *transition paths for the corresponding trajectories from (a) Delta-low to Delta-high cell and (b) Delta-high to Delta-low cell. Thus, the regions shaded in orange indicate the transition tubes around the MAPs (indicated by the dotted magenta lines) for the corresponding noise level. Representative stochastic sample paths (identical to the ones shown in Figure 5) obtained by simulating the full stochastic CTMC model (Table SM2) with the system sizes (a)* $\Omega = 70$*, (b)* $\Omega = 450$*, are plotted in black. The thin grey lines indicate streamlines of the corresponding mean-field system (Equation (SM1.2)). The Delta-high (Delta-low) cell stable steady state is indicated by a green (red) filled circle; the unstable saddle by a blue unfilled circle. The plots represent three-dimensional projections of the full five-dimensional system as defined by Equation (SM1.2). Parameter values are fixed as indicated in Table SM3.*

Algorithm SM5.1 Pseudocode algorithm for simulating the multi-agent CG model of a system with a region of multistability.

Specify final simulation time, T_{final}, and the system size, Ω.
Given a discretisation, $\{v_j\}_j$, of the external (bifurcation) variables, read look-up tables for steady states, quasipotential and prefactor values.
For each v_j, compute CG transition rates, $k_{x_s \to x_l}$, $s,\ l = 1 \dots S,\ s \neq l$, defined by Equation (3.1) for the specified Ω. Here $\{x_s\}_{s=1}^{S}$ is a set of stable steady states.
Initialise interpolation routines to establish an input-output relationship between an arbitrary $v \in \mathcal{V}$ and the CG transition rates, $k_{x_s \to x_l}$.
Initialise the system with a pre-pattern by using the original stochastic model or its mean-field limit (preferable).
Set the simulation time, $t = 0$.
while $t < T_{final}$ **do**
    Set total propensity, $P = 0$.
    for each entity, e, **do**
        Compute its external variables, v^e.
        for $s,\ l = 1 \dots S,\ s \neq l$, **do**
            Interpolate $k^e_{x_s \to x_l}$ for the given v^e.
            $P = P + k^e_{x_s \to x_l}$.
        end for
    end for
    Sample the waiting time for the next transition to occur, $\bar{\tau} \sim \text{Exp}(1/P)$, where $\text{Exp}(\lambda)$ is an exponential distribution of intensity λ.
    Probabilistically (as in the Gillespie algorithm), decide which transition occurs (in which entity, $\bar{e}$, and between which stable steady states).
    For this entity, compute again $v^{\bar{e}}$ and interpolate its new steady state after the transition.
    Update the simulation time, $t = t + \bar{\tau}$.
end while
End of simulation.

SM5. Pseudocode algorithm for simulating the multi-agent CG model of a system with a region of multistability.

SM6. Quantification metrics. We used the following metrics to compare our models.

Delta-high cell proportion. In the angiogenesis model [SM9], we used Delta levels as a proxy to determine cell phenotype. Thus, the number of Delta-high cells is given by the number of cells whose Delta level exceeds the threshold $d_{tip} = 0.1\beta_D$. Then the Delta-high cell proportion at time, t, can be computed as the ratio of the number of Delta-high cells to the total number of cells. Here, β_D is the characteristic expression of Delta in a cell (see Table SM3).

Delta-high cell cluster distribution. Depending on the parameter values, in the final spatial pattern (at a fixed final simulation time), Delta-high cells can form small clusters, i.e. be adjacent (see Figure SM5). We extracted the distribution of the cluster sizes for final configurations of the spatial phenotype pattern.

Computational cost. Computational cost is defined to be the mean CPU times (in seconds) required to perform a single realisation of a model simulation. Technical specifications of computers used to perform the simulations are indicated in File S1.

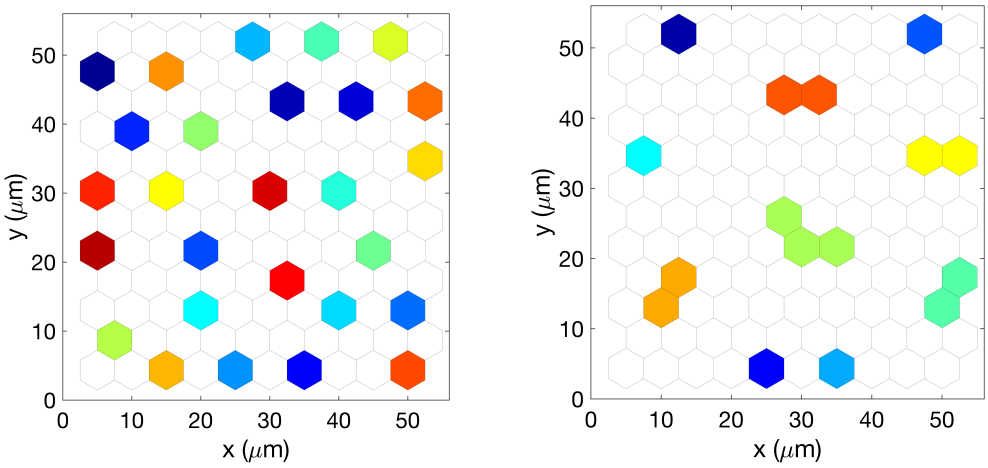

(a) (b)

FIG. SM5. ***Simulation results showing how the long time distribution of Delta-high cell clusters in a small monolayer of cells changes as the cell-to-cell interaction radius varies.*** *Cell interaction radius (a) $R_s = 5\mu m$ (b) $R_s = 15\mu m$. Each group of Delta-high cells (a cluster) is coloured by a distinct colour (randomly chosen). Delta-low cells are left white.*

SM7. Supplementary figures, tables.

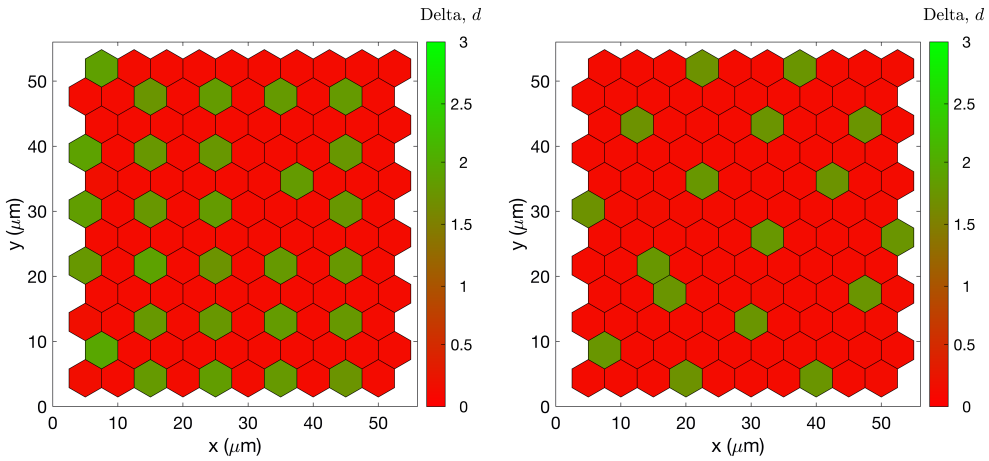

(a) $R_s = 5\mu m$ (b) $R_s = 10\mu m$

(c) $R_s = 15\mu m$ (d) $R_s = 20\mu m$

FIG. SM6. ***A series of plots showing how the spatial patterns, generated by the VEGF-Delta-Notch signalling in a cell monolayer, become more clustered as the interaction radius, R_s, increases.*** *For these simulations, the interaction radius is fixed at (a) $R_s = 5\mu m$; (b) $R_s = 10\mu m$; (c) $R_s = 15\mu m$; (d) $R_s = 20\mu m$. The system size is fixed at, $\Omega = 100$; the rest of the parameter values were fixed as indicated in Table SM3. The colour bar indicates the levels of Delta, d, in each cell.*

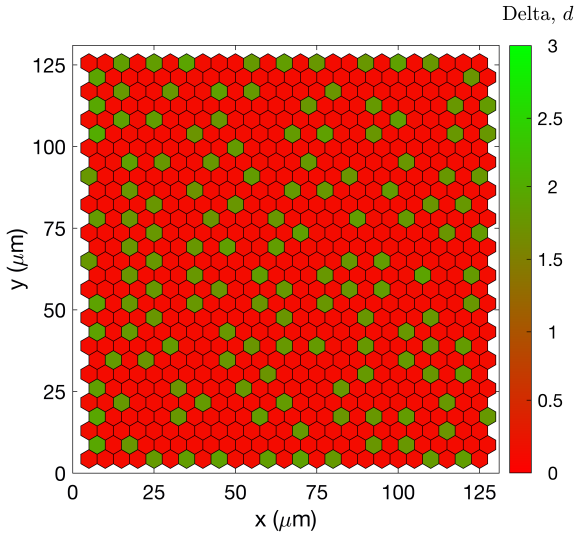

FIG. SM7. ***Initial configuration of a cell monolayer for numerical simulation.*** *The size of the monolayer is* 25×29 *voxels. The colour bar indicates the initial levels of Delta, d, in each cell.*

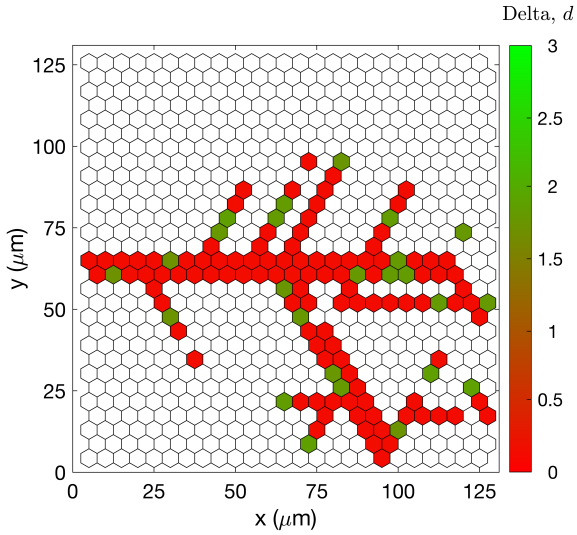

FIG. SM8. ***Initial setup configuration of a branching network for numerical simulation.*** *We extracted this configuration from a simulation of the angiogenesis model [SM9]. The colour bar indicates the level of Delta, d. Voxels without cells are left white in the plot.*

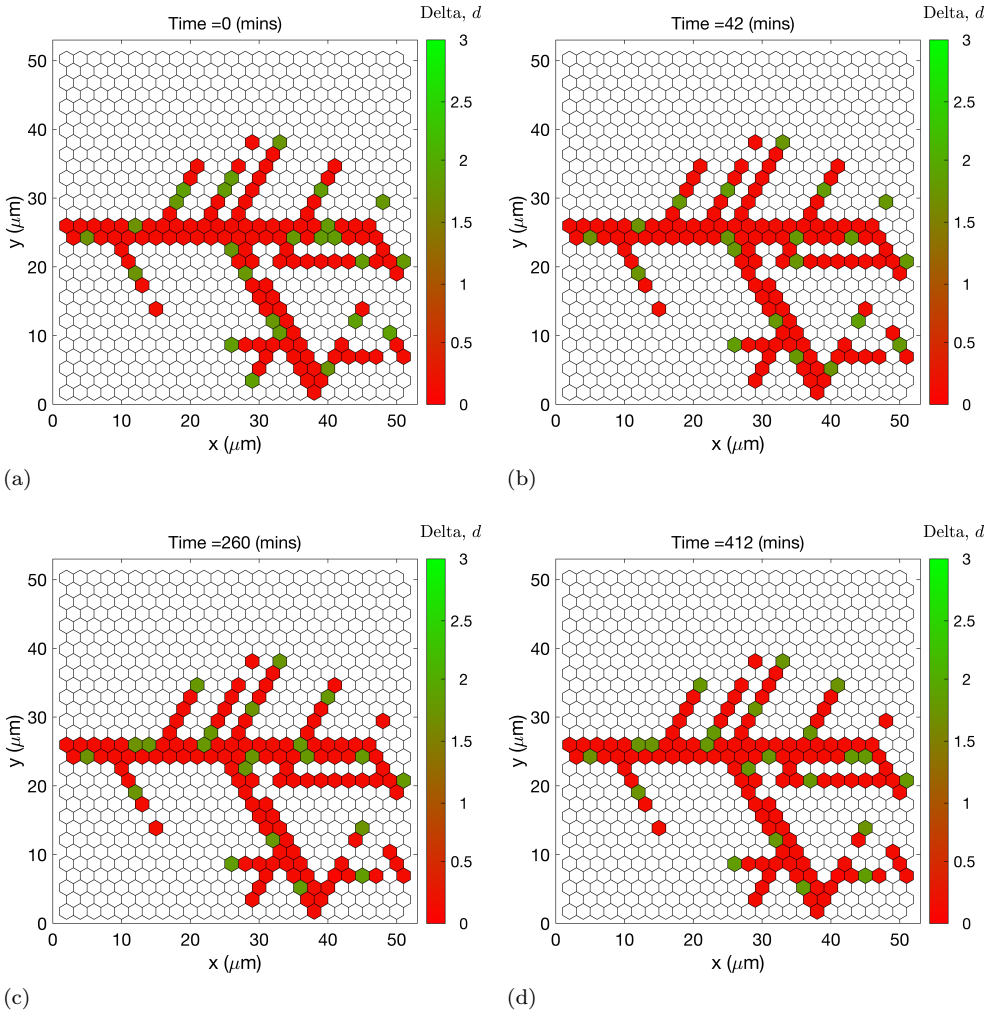

FIG. SM9. ***A series of plots illustrating the time evolution of the phenotype patterning in a branching network in a typical simulation of the CG system for the multicellular VEGF-Delta-Notch signalling pathway.*** *Time points (indicated in the title of each plot) are (a)* $t = 0$*, (b)* $t = 42$*, (c)* $t = 260$*, (d)* $t = 412$ *minutes. The colour bar indicates the levels of Delta, d, in each cell. For these simulations, the interaction radius and system size were fixed at* $R_s = 15\mu m$ *and* $\Omega = 100$*, respectively. The remaining parameter values were fixed as indicated in Table* SM3.

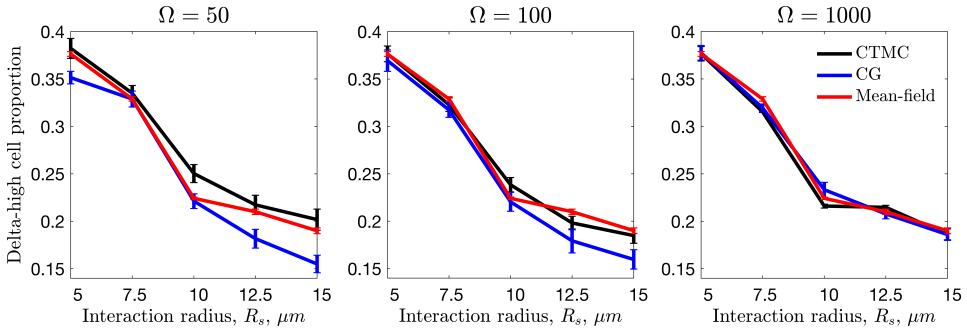

(a)

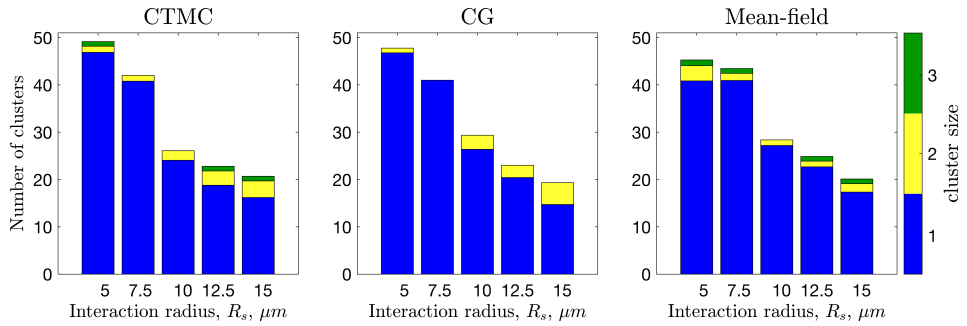

(b)

FIG. SM10. ***Comparison of the dynamics of the multicellular VEGF-Delta-Notch model simulated on a branching network using the full stochastic (CTMC), CG, and mean-field descriptions.*** *(a) The Delta-high cell proportion as a function of the cell-to-cell interaction radius, R_s, for varying noise amplitude, $\epsilon = 1/\Omega$ (the value of Ω is indicated in the title of each plot), for the full stochastic CTMC (black), CG (blue) and mean-field (red) descriptions. (b) A series of barplots showing how the long-time distribution of Delta-high cell clusters changes as the interacton radius, R_s, varies for the full stochastic CTMC (left panel), CG (middle panel), and mean-field (right panel) systems. The number of single Delta-high cells in the final pattern (i.e. at a fixed final simulation time) is shown in blue; the number of clusters with 2, and 3 adjacent Delta-high cells is shown in yellow and green, respectively. For these simulations, we fixed $\Omega = 1000$ ($\epsilon = 0.001$). The results are averaged over 100 realisations. The remaining parameter values were fixed as indicated in Table SM3.*

TABLE SM3
Non-dimensional parameters of the VEGF-Delta-Notch system.

Parameter	**Value**
β_N	2.5, fixed in all figures.
β_D	4.0, fixed in all figures.
β_{R_2}	4.0, fixed in all figures.
ρ_N	20.0, fixed in all figures.
ρ_{R_2}	10.0, fixed in all figures.
$\lambda_{I,N}$	4.0, fixed in all figures.
λ_{I,R_2}	0.0, fixed in all figures.
$\lambda_{R_2^*,D}$	2.0, fixed in all figures.
n_N	2, fixed in all figures.
n_D	1, fixed in all figures.
n_{R_2}	1, fixed in all figures.
η	0.5, fixed in all figures.
τ	5.0, fixed in all figures.
κ	4.0 for Figures SM3 and 5 to 7; 12.0 for all other figures and simulations.
v_{ext}	0.1 for Figures SM3 and 5 to 7; 1.25 for all other figures and simulations.
d_{ext}	0.2 for Figures SM3 and 5 to 7; $d_{ext} \in [0.0, 4.0]$ and the exact value is determined during the simulations (depending on the neighbourhood of each cell) for all other figures.
n_{ext}	0.5 for Figures SM2a, SM3, and 5 to 7; $d_{ext} \in [0.0, 4.0]$ and the exact value is determined during the simulations (depending on the neighbourhood of each cell) for all other figures.
voxel width, h	5 μm in all multicellular simulations (hexagon width).
R_s	15 μm in Figures SM9, 11, and 12; for all other multicellular simulations R_s is indicated in the text and/or figure captions.
final simulation time, T_{final}	12000 mins for Figures SM6 and 11; $5 \cdot 10^{23}$ mins for Figure 12; 1500 mins for Figures SM10, 13, and 14; 9000 mins for Figure SM9.

REFERENCES

[SM1] R. Blanco and H. Gerhardt, *Vegf and notch in tip and stalk cell selection*, Cold Spring Harbor Perspectives in Medicine, 3 (2013), p. a006569.

[SM2] M. Boareto, M. K. Jolly, M. Lu, J. N. Onuchic, C. Clementi, and E. Ben-Jacob, *Jagged–delta asymmetry in notch signaling can give rise to a sender/receiver hybrid phenotype*, Proceedings of the National Academy of Sciences, 112 (2015), pp. E402–E409.

[SM3] J. Elf and M. Ehrenberg, *Spontaneous separation of bi-stable biochemical systems into spatial domains of opposite phases*, Systems Biology, 1 (2004), pp. 230–236.

[SM4] H. Gerhardt, M. Golding, M. Fruttiger, C. Ruhrberg, A. Lundkvist, A. Abramsson, M. Jeltsch, C. Mitchell, K. Alitalo, D. Shima, et al., *Vegf guides angiogenic sprouting utilizing endothelial tip cell filopodia*, The Journal of Cell Biology, 161 (2003), pp. 1163–1177.

[SM5] D. T. Gillespie, *A general method for numerically simulating the stochastic time evolution of coupled chemical reactions*, Journal of Computational Physics, 22 (1976), pp. 403–434.

[SM6] T. Grafke, T. Schäfer, and E. Vanden-Eijnden, *Long term effects of small random perturbations on dynamical systems: Theoretical and computational tools*, in Recent Progress and Modern Challenges in Applied Mathematics, Modeling and Computational Science, Springer, 2017, pp. 17–55.

[SM7] M. Heymann and E. Vanden-Eijnden, *The geometric minimum action method: A least action principle on the space of curves*, Communications on Pure and Applied Mathematics: A Journal Issued by the Courant Institute of Mathematical Sciences, 61 (2008), pp. 1052–1117.

[SM8] L. Jakobsson, C. A. Franco, K. Bentley, R. T. Collins, B. Ponsioen, I. M. Aspalter, I. Rosewell, M. Busse, G. Thurston, A. Medvinsky, et al., *Endothelial cells dynamically compete for the tip cell position during angiogenic sprouting*, Nature cell biology, 12 (2010), p. 943.

[SM9] D. Stepanova, H. M. Byrne, P. K. Maini, and T. Alarcón, *A multiscale model of complex endothelial cell dynamics in early angiogenesis*, PLOS Computational Biology, 17 (2021), p. e1008055.

[SM10] M. Tao, *Hyperbolic periodic orbits in nongradient systems and small-noise-induced metastable transitions*, Physica D: Nonlinear Phenomena, 363 (2018), pp. 1–17.

[SM11] B. Ubezio, R. A. Blanco, I. Geudens, F. Stanchi, T. Mathivet, M. L. Jones, A. Ragab, K. Bentley, and H. Gerhardt, *Synchronization of endothelial dll4-notch dynamics switch blood vessels from branching to expansion*, Elife, 5 (2016), p. e12167.